

Supplementary Information

Green iodination of arenes using sulphated ceria-zirconia catalysts in polyethylene glycol

Sandeep S. Kahandal,^a Sandip R. Kale,^a Manoj B. Gawande,^{*b} Radek Zboril,^b Rajender S. Varma,^{*c} and Radha V. Jayaram^{*a}

^aDepartment of Chemistry, Institute of Chemical Technology (Autonomous), N. Parekh Marg, Matunga, Mumbai 400 019, India,

Email: rv.jayaram@ictmumbai.edu.in; Fax +91(22)24145614

^bRegional Centre of Advanced Technologies and Materials, Faculty of Science, Department of Physical Chemistry, Palacky University, Olomouc, 17. listopadu 12, 771 46 Olomouc, Czech Republic

Email- mbgawande@yahoo.co.in

^cSustainable Technology Division, National Risk Management Research Laboratory, US Environmental Protection Agency, MS 443, 26 West Martin Luther King Drive, Cincinnati, Ohio, 45268, USA

Email: Varma.Rajender@epamail.epa.gov

No	Contents	Page No
A)	Experimental	2
B)	Characterization data of Catalyst	3-12
C)	UV-Vis spectra of I ₂ +PEG	13
D)	Mass spectra	15-26
E)	References	27

A) Experimental

a) Catalyst preparation:

All chemicals were of analytical grade and were used without any further purification. The $\text{SO}_4^{2-}/\text{Ce}_x\text{Zr}_{1-x}\text{O}_2$ were prepared by the method described by Lee et al.¹⁻² Precipitate of $\text{Zr}(\text{OH})_4$ was obtained by adding aqueous ammonia into an 0.25 M solution of zirconium oxychloride at room temperature with vigorous stirring until the pH of the mother liquor reached at 8. The preparation of catalyst doped with Ce and modified with sulphate simultaneously was carried out by adding an acidic aqueous solution of cerium sulphate ($\text{Ce}(\text{SO}_4)_2 \cdot 4\text{H}_2\text{O}$) to the $\text{Zr}(\text{OH})_4$ followed by drying at 110°C for 24 h and calcined at 650°C for 2 h. The series of catalysts were prepared by varying mol % of cerium (0.02-0.25) added in the catalyst.

b) Typical experimental procedure:

In typical reaction procedure of iodination, aniline (2 mmol), molecular iodine (2 mmol) were taken in 25 mL round bottom flask. $\text{SO}_4^{2-}/\text{Ce}_{0.07}\text{Zr}_{0.93}\text{O}_2$ (15 wt %) with 2 mL PEG-200 were added to it. The reaction mixture was stirred for 12 h at room temperature (30 °C). The reaction was continuously monitored by using TLC and gas chromatography. After completion of reaction, 10 mL of ethyl acetate was added to the reaction mass and catalyst was separated by simple filtration. The resulting reaction mass was treated with $\text{Na}_2\text{S}_2\text{O}_3$ solution (10 mL) and extracted with ethyl acetate (10 mL). The reaction mixture was then passed through a bed of anhydrous Na_2SO_4 . Evaporation of the solvent afforded the iodo compound, which was purified by column chromatography on silica gel using a mixture of hexane/EtOAc (80:20). All the structures were confirmed by GC-MS.

B) Characterization data of the catalysts

a) FT-IR of the $\text{SO}_4^{2-}/\text{Ce}_x\text{Zr}_{(1-x)}\text{O}_2$

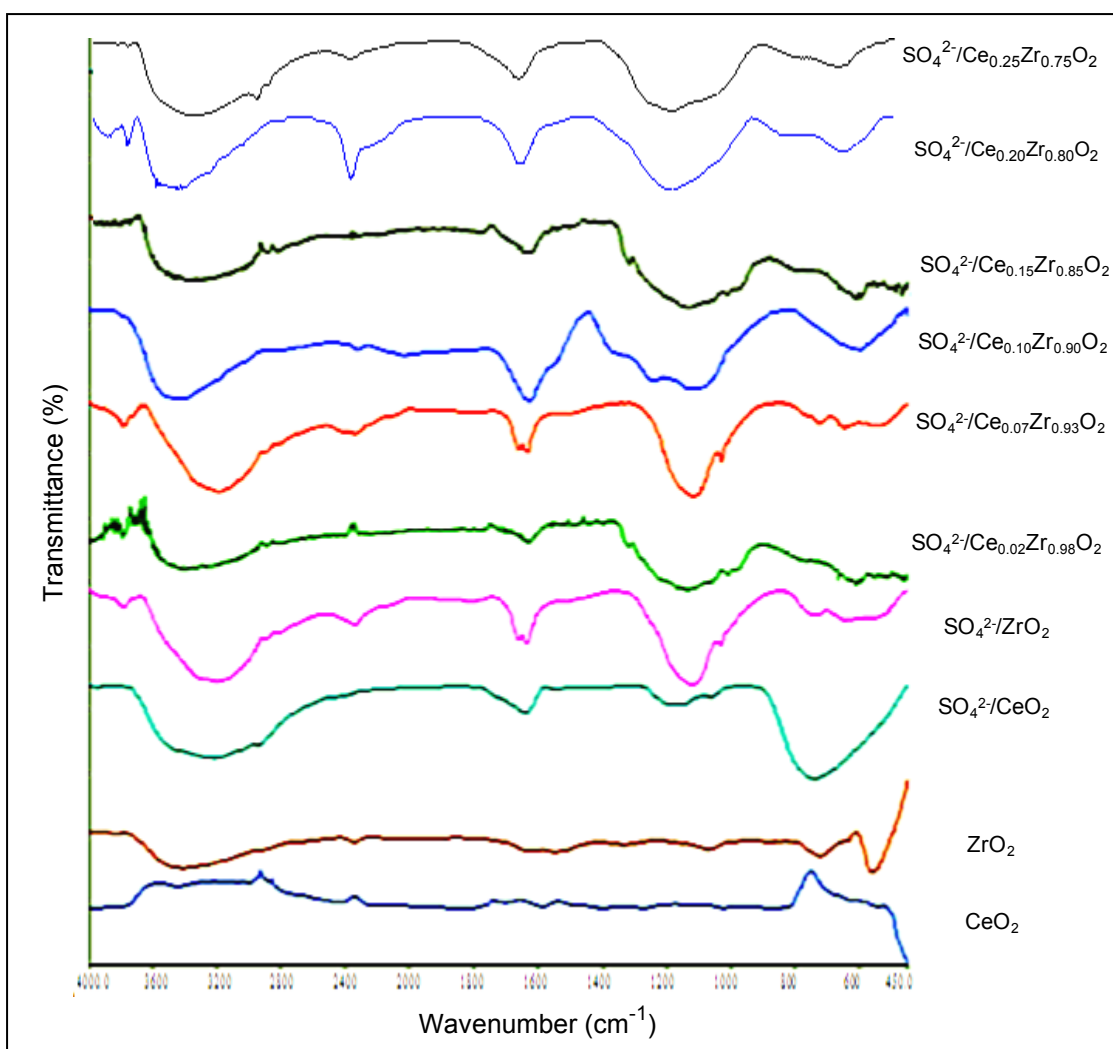
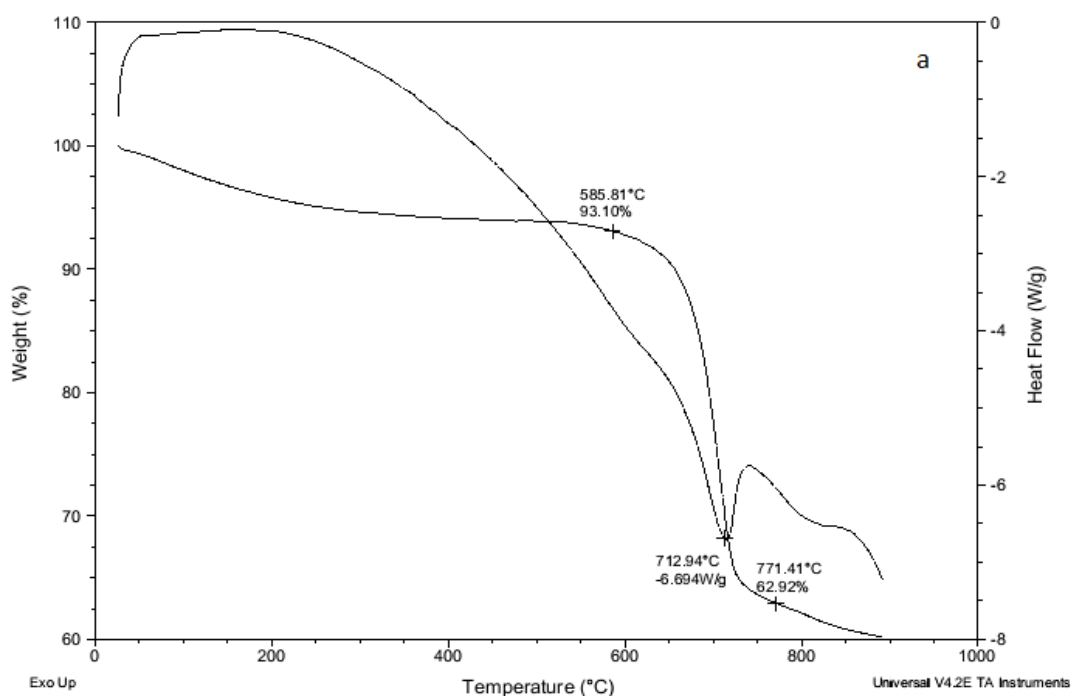


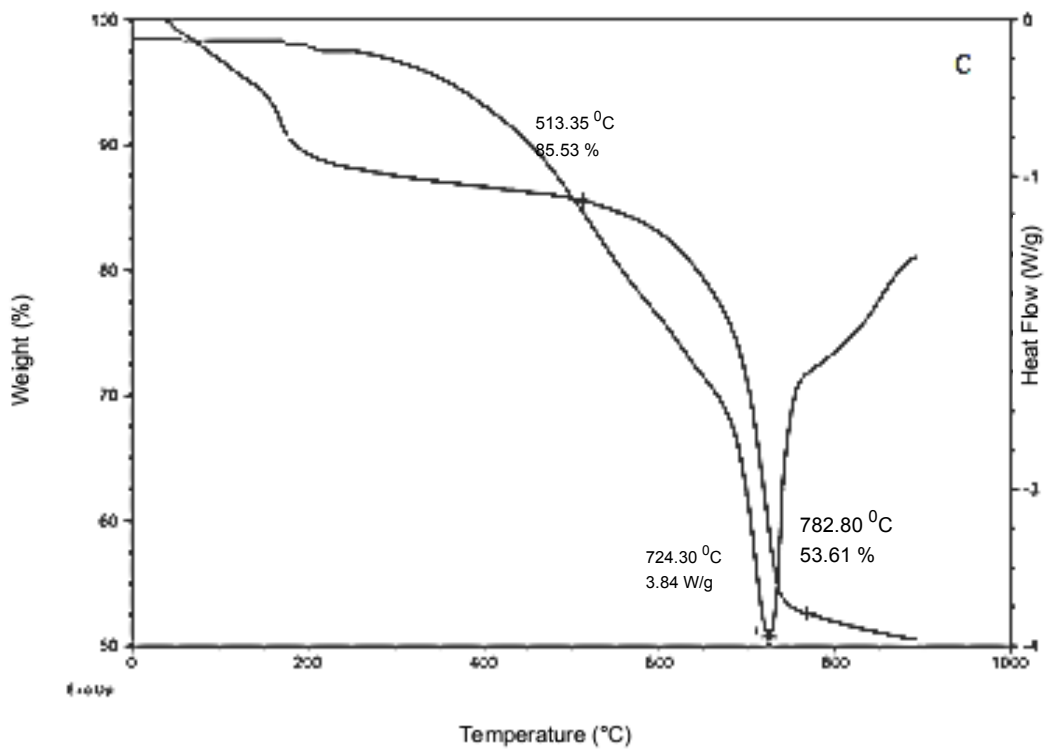
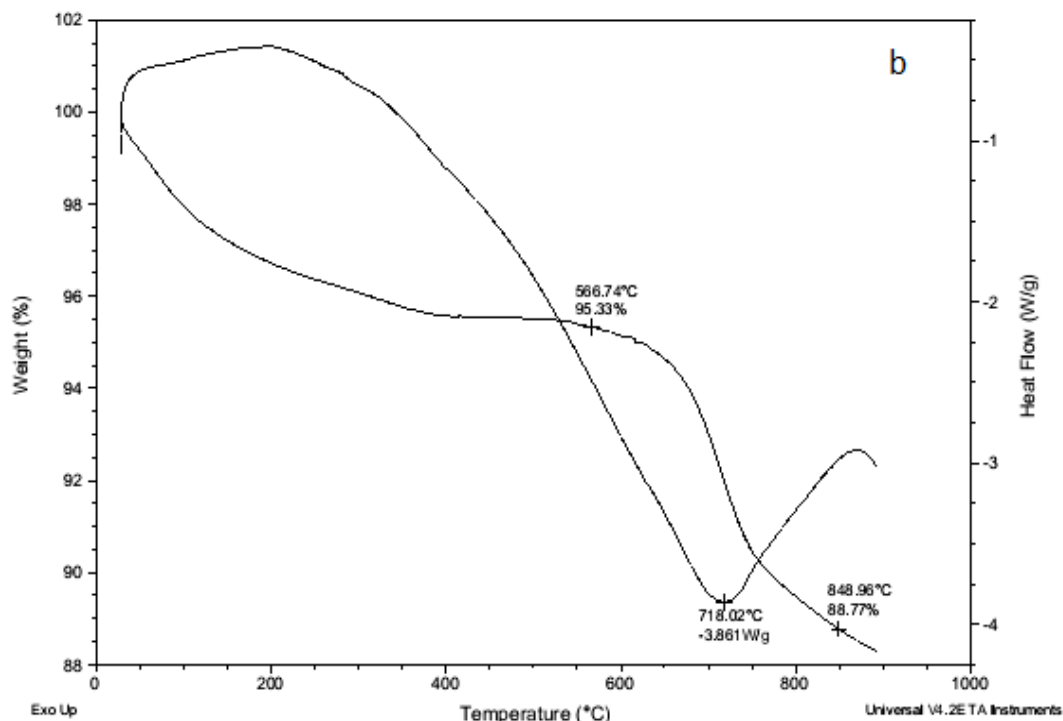
Figure 1. FT-IR spectra of $\text{SO}_4^{2-}/\text{Ce}_x\text{Zr}_{(1-x)}\text{O}_2$ catalysts.

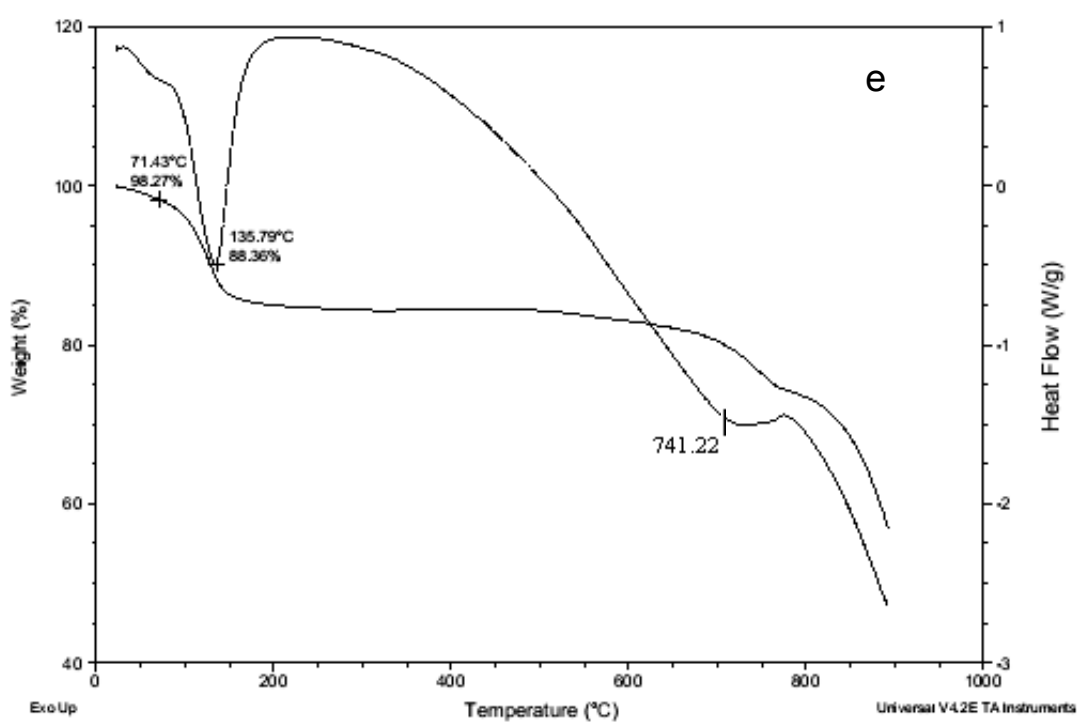
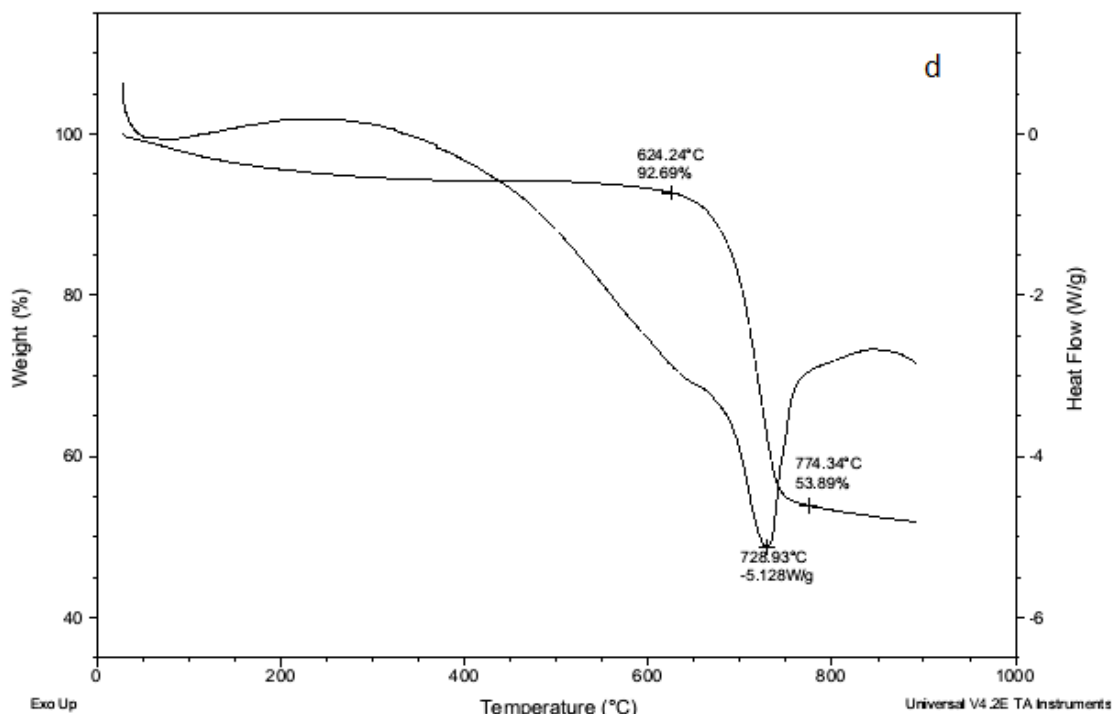
FT-IR spectra were recorded for confirming the presence of sulphate ion units on the surface of ceria-zirconia. The intense absorption bands at around 1250, 1222, 1142 and 1096 cm^{-1} are assigned to the S-O stretching frequency region for bidentate sulphate ions coordinated to the metal. The former and the latter two bands are assigned to asymmetric and symmetric stretching vibrations of the O=S=O and O-S-O groups respectively. The bands at 1625 and 1635 cm^{-1} are assigned to the deformation vibration modes of the adsorbed water.¹ These characteristic bands of bidentate sulphate ions are absent in

unsulfated ZrO_2 and CeO_2 . In sulphated zirconia IR absorption bands were observed at the same region as that of the $\text{SO}_4^{2-}/\text{Ce}_x\text{Zr}_{1-x}\text{O}_2$. In sulphated ceria, slight shift of absorption bands at 1300, 1143, 1196 and 1056 cm^{-1} was observed.

b) TGA-DSC curve of $\text{SO}_4^{2-}/\text{Ce}_x\text{Zr}_{(1-x)}\text{O}_2$ catalysts







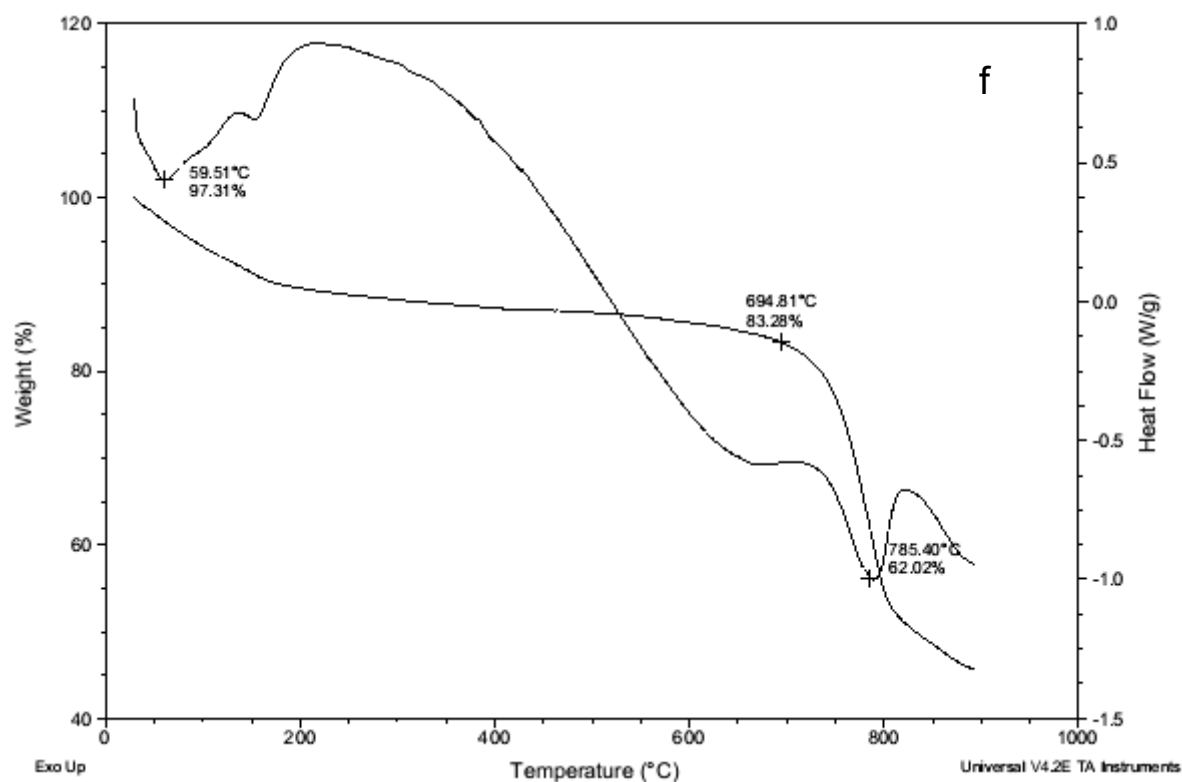


Figure 2. DSC-TGA curve of a) $\text{SO}_4^{2-}/\text{Ce}_{0.02}\text{Zr}_{0.98}\text{O}_2$ (b) $\text{SO}_4^{2-}/\text{Ce}_{0.07}\text{Zr}_{0.93}\text{O}_2$ (c) $\text{SO}_4^{2-}/\text{Ce}_{0.10}\text{Zr}_{0.90}\text{O}_2$ (d) $\text{SO}_4^{2-}/\text{Ce}_{0.15}\text{Zr}_{0.85}\text{O}_2$ (e) $\text{SO}_4^{2-}/\text{Ce}_{0.20}\text{Zr}_{0.80}\text{O}_2$ (f) $\text{SO}_4^{2-}/\text{Ce}_{0.25}\text{Zr}_{0.75}\text{O}_2$

Thermal stability of $\text{SO}_4^{2-}/\text{Ce}_x\text{Zr}_{1-x}\text{O}_2$ ($x = 0.2-0.25$) catalysts was investigated by DSC-TGA thermal analysis. The first weight loss for all the compositions occurs below 200 °C which is due to the loss of physically adsorbed water. The catalysts exhibit good thermal stability and no remarkable weight loss was observed further upto 700 °C. Next prominent weight loss of the catalysts occurs at 700 °C to 900 °C mainly due to decomposition of sulphate species with the evolution of SO_3 (a-f). The endothermic peaks at 712–785 °C observed in the case of $\text{SO}_4^{2-}/\text{Ce}_x\text{Zr}_{1-x}\text{O}_2$ ($x=0.2-0.25$) samples are due to the evolution of SO_3 from sulphate species bonded to the surface of Ce-doped ZrO_2 . The decomposition temperature depends on the amount of Ce and sulphate species present in the catalyst. The decomposition temperature increases (713-785 °C) with increasing Ce content from 0.02-25 mol%, resulting in increased thermal stability of the surface sulphate species.

c) XRD of the Catalysts:

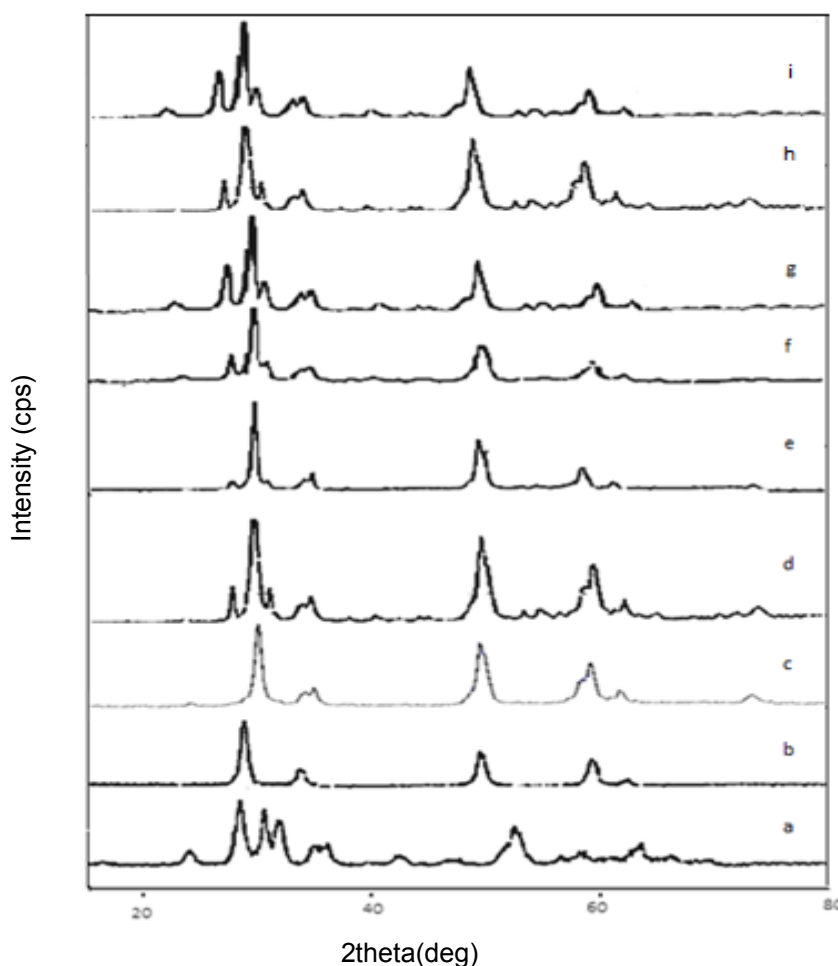


Figure 3. XRD patterns of (a) ZrO₂, (b) CeO₂, (c) SO₄²⁻/ZrO₂, (d) SO₄²⁻/Ce_{0.02}Zr_{0.98}O₂, (e) SO₄²⁻/Ce_{0.07}Zr_{0.93}O₂, (f) SO₄²⁻/Ce_{0.10}Zr_{0.90}O₂, (g) SO₄²⁻/Ce_{0.15}Zr_{0.85}O₂ (h) SO₄²⁻/Ce_{0.20}Zr_{0.80}O₂ (i) SO₄²⁻/Ce_{0.25}Zr_{0.75}O₂

The XRD patterns of sulphated metal oxides and mixed metal oxides with different Ce content are shown in **figure 3**. All the samples were crystalline in nature, wherein CeO₂ forms a solid solution with ZrO₂.¹⁻² SO₄²⁻/Ce_xZr_{1-x}O₂ ($x = 0.02\text{--}0.25$ mol%) show characteristics peaks of catalytically active tetragonal phase ($2\theta = 30.18^\circ$ (with 100 as relative intensity) and the peaks located at 34.616° , 35.283° , 50.214° , 50.770° , 59.291° , 60.187° , 62.724° and 74.617°) [d-i]. The oxide of cerium (CeO₂) shows characteristic peaks of fluorite phase whereas ZrO₂ was present in both tetragonal and monoclinic phases (a-b). Sulphated zirconia shows characteristic peaks of tetragonal phase which is supposed to be the catalytically active phase (c). **d)** BET surface area and number and relative strength of acid sites by potentiometric method^a

Table 1. BET surface area and number and relative strength of acid sites by potentiometric method^a with conversion and selectivity

Catalyst	BET Surface area (m ² .g ⁻¹)	Acidity (mmol/g) ^b	E _i (mV) ^c	Conversion (%)	Selectivity (%) ^d
ZrO ₂	12	0.8	55	60	93/7
CeO ₂	10	0.3	27	45	91/9
SO ₄ ²⁻ /ZrO ₂	37	2.07	168	84	96/4
SO ₄ ²⁻ /CeO ₂	23	1.22	154	54	85/15
Ce _{0.07} Zr _{0.93} O ₂	17	1.54	157	43	100
SO ₄ ²⁻ /CeO ₂ + SO ₄ ²⁻ /ZrO ₂	-	-	-	65	88/12
SO ₄ ²⁻ /Ce _{0.02} Zr _{0.98} O ₂	22	3.17	440	80	100
SO ₄ ²⁻ /Ce _{0.07} Zr _{0.93} O ₂	53	4.23	560	100	100
SO ₄ ²⁻ /Ce _{0.10} Zr _{0.90} O ₂	28	3.52	450	82	100
SO ₄ ²⁻ /Ce _{0.15} Zr _{0.85} O ₂	14	3.50	460	62	98/2
SO ₄ ²⁻ /Ce _{0.20} Zr _{0.80} O ₂	12	2.97	248	57	95/5
SO ₄ ²⁻ /Ce _{0.25} Zr _{0.75} O ₂	10	2.17	197	53	95/5
SO ₄ ²⁻ /Y _{0.04} Zr _{0.96} O ₂	34	1.23	148	56	92/8
SO ₄ ²⁻ /Y _{0.08} Zr _{0.92} O ₂	43	1.64	195	54	90/10
SO ₄ ²⁻ /Y _{0.12} Zr _{0.88} O ₂	52	1.93	310	68	90/10
SO ₄ ²⁻ /Y _{0.16} Zr _{0.84} O ₂	75	4.19	530	92	94/6
SO ₄ ²⁻ /Y _{0.20} Zr _{0.80} O ₂	35	2.91	330	69	99/1
SO ₄ ²⁻ /Y _{0.24} Zr _{0.76} O ₂	29	2.65	248	60	100

^aSulphated ceria-zirconia catalysts are calcined at 650 °C for 2 h. ^bTotal number of acid sites determined by n-butylamine potentiometric titration, ^cE_i- Initial electrode potential (mV). ^d(%) Selectivity, para/ortho isomers for iodoaniline synthesis.

BET surface areas of the as synthesized $\text{SO}_4^{2-}/\text{Ce}_x\text{Zr}_{1-x}\text{O}_2$ ($X=0.02-0.25$) catalysts were determined (**Table 1**). The results indicate that both the surface area and acidity (**Figure 4**) are dependent on Ce: Zr ratio of the catalyst. $\text{SO}_4^{2-}/\text{Ce}_{0.07}\text{Zr}_{0.93}\text{O}_2$ has the highest surface area as compared to other compositions of $\text{SO}_4^{2-}/\text{Ce}_x\text{Zr}_{1-x}\text{O}_2$.

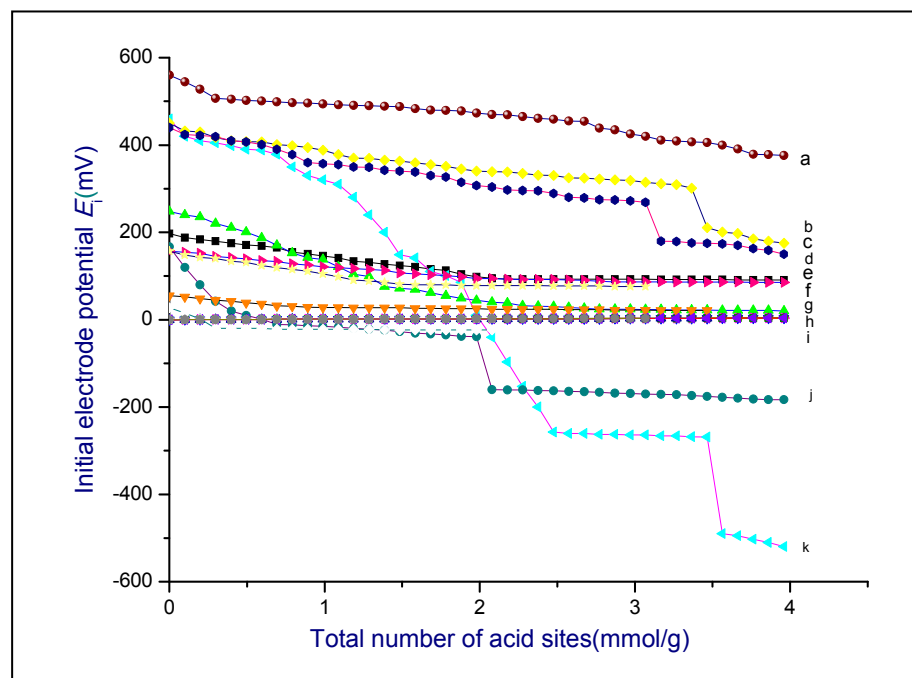


Figure 4. Potentiometric titration curves for (a) $\text{SO}_4^{2-}/\text{Ce}_{0.02}\text{Zr}_{0.98}\text{O}_2$ (b) $\text{SO}_4^{2-}/\text{Ce}_{0.07}\text{Zr}_{0.93}\text{O}_2$ (c) $\text{SO}_4^{2-}/\text{Ce}_{0.10}\text{Zr}_{0.90}\text{O}_2$ (d) $\text{SO}_4^{2-}/\text{Ce}_{0.25}\text{Zr}_{0.85}\text{O}_2$ (e) $\text{SO}_4^{2-}/\text{CeO}_2$ (f) $\text{Ce}_{0.07}\text{Zr}_{0.93}\text{O}_2$ (g) ZrO_2 (h) $\text{SO}_4^{2-}/\text{Ce}_{0.20}\text{Zr}_{0.80}\text{O}_2$ (i) CeO_2 (j) $\text{SO}_4^{2-}/\text{ZrO}_2$ (k) $\text{SO}_4^{2-}/\text{Ce}_{0.15}\text{Zr}_{0.85}\text{O}_2$

d) Surface morphology of $\text{SO}_4^{2-}/\text{Ce}_{0.07}\text{Zr}_{0.93}\text{O}_2$ catalyst

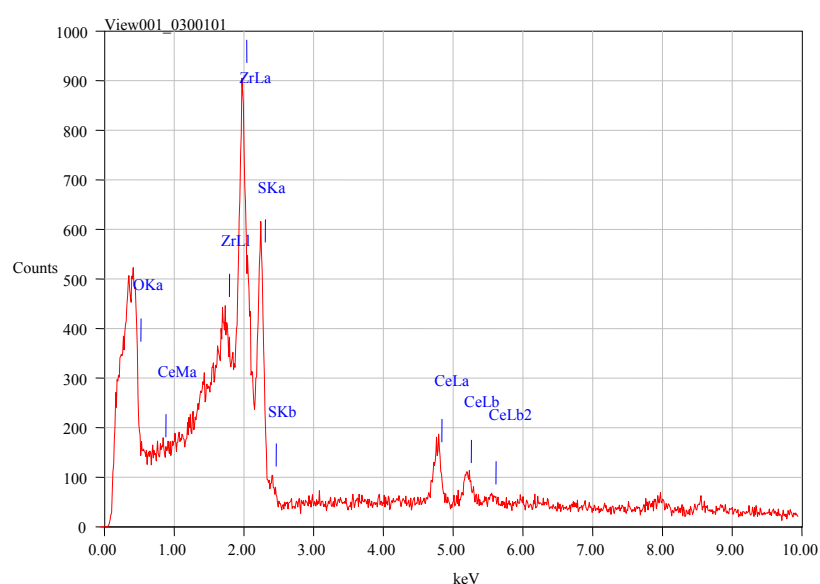
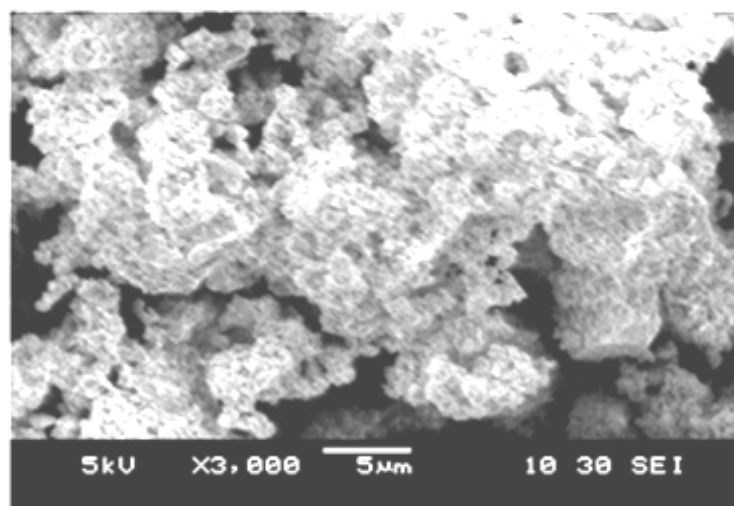


Figure 5. SEM-EDX analysis of $\text{SO}_4^{2-}/\text{Ce}_{0.07}\text{Zr}_{0.93}\text{O}_2$ composition

SEM images were recorded using a Tungsten source on JEOL model JSM-6390 instrument. EDX-XAF analysis showed 7 mol% of Ce and 93.0 mol% of Zr in case of $\text{SO}_4^{2-}/\text{Ce}_{0.07}\text{Zr}_{0.93}\text{O}_2$. The results are in well agreement with the calculations and minimal difference was observed (**Figure 5**).

Table 2. Surface ratio of Ce/Zr and surface density of sulphate for $\text{SO}_4^{2-}/\text{Ce}_x\text{Zr}_{1-x}\text{O}_2$

No	BET Surface area ($\text{m}^2\cdot\text{g}^{-1}$)	Catalyst	Ce/Zr	Surface density of sulphate
1	22	$\text{SO}_4^{2-}/\text{Ce}_{0.02}\text{Zr}_{0.98}\text{O}_2$	0.020	3.3
2	53	$\text{SO}_4^{2-}/\text{Ce}_{0.07}\text{Zr}_{0.93}\text{O}_2$	0.075	8.1
3	28	$\text{SO}_4^{2-}/\text{Ce}_{0.10}\text{Zr}_{0.90}\text{O}_2$	0.111	7.2
4	14	$\text{SO}_4^{2-}/\text{Ce}_{0.15}\text{Zr}_{0.85}\text{O}_2$	0.176	5.5
5	12	$\text{SO}_4^{2-}/\text{Ce}_{0.20}\text{Zr}_{0.80}\text{O}_2$	0.25	5.2
6	10	$\text{SO}_4^{2-}/\text{Ce}_{0.25}\text{Zr}_{0.75}\text{O}_2$	0.333	5.0

Ce/Zr and surface density of sulphate were determined by EDAX method.

The surface ratio (Ce/Zr) 0.075 showed highest surface density of sulphate in sulphated ceria-zirconia. The highest surface density of sulphate resulted in the increase of total number of acidic sites for $\text{SO}_4^{2-}/\text{Ce}_{0.07}\text{Zr}_{0.93}\text{O}_2$ composition. For all the other compositions, the surface densities of sulphate were found to be lower and the total numbers of acid sites are also low.

C) (UV-Vis spectra of I₂+PEG).

The value of $\lambda_{\text{max}} = 360 \text{ nm}$ for the diatomic I₂ state and whose interatomic distance is a little prolonged by the interaction with solvent molecules³ (PEG-200,400,600 (b to d). The intensity of $\lambda_{\text{max}} = 360 \text{ nm}$ for I₂+Ethanol is very small (e).

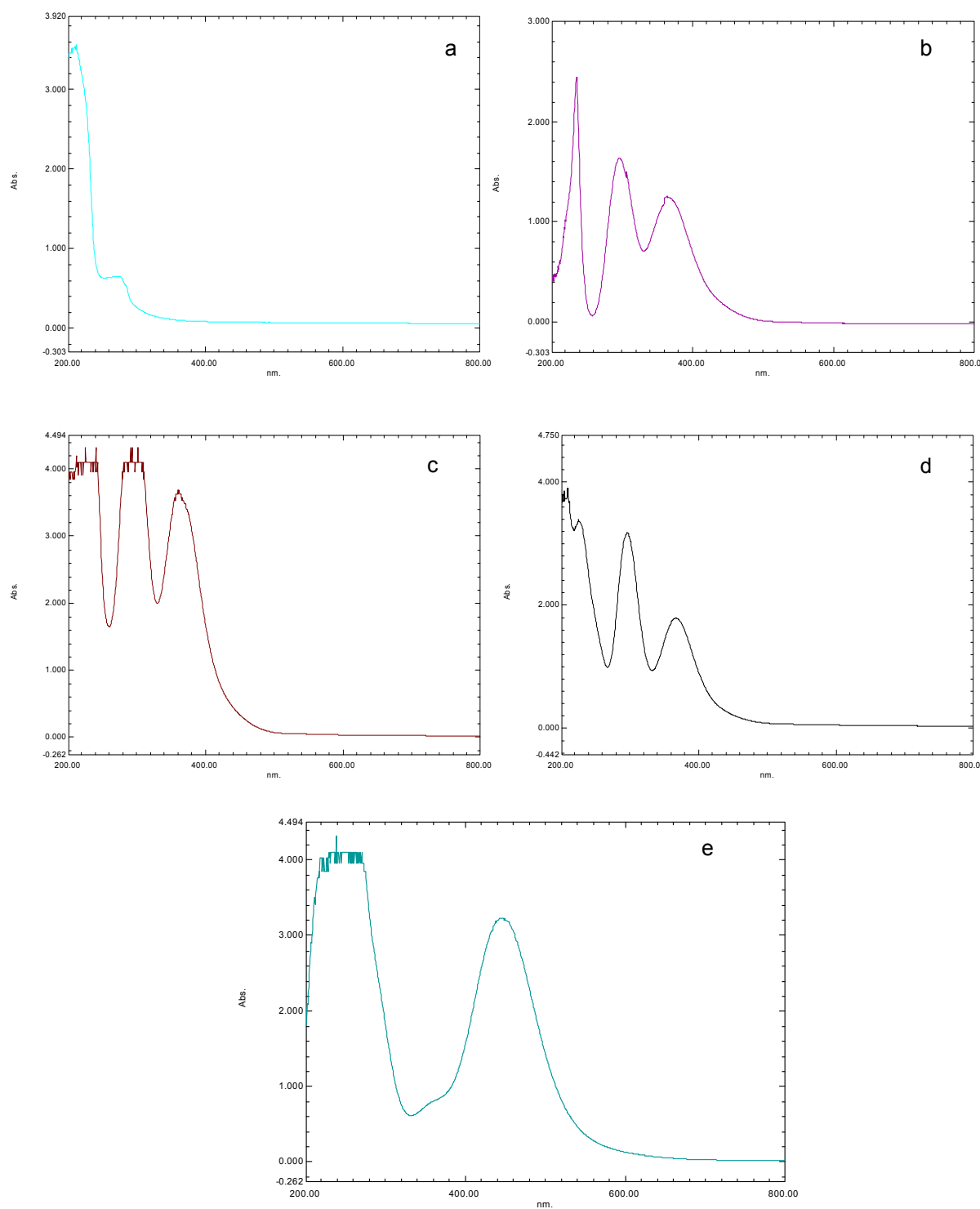


Figure 6, U.V-Vis spectra for (a) PEG-200 (b) I₂+PEG-200 (c) I₂+PEG-400 (d) I₂+PEG-600 (e) I₂+Ethanol

D) Spectral data:

4-Iodo-aniline (Figure 7)

GC-MS (EI, 70 eV): m/z (%) = 219 (100 %) [M^+], 127 (3 %), 109 (10 %), 92 (51 %), 65 (50 %), 52 (5 %)

2, 4-Diiodoaniline (Figure 8)

GC-MS (EI, 70 eV): m/z (%) = 345 (100 %) [M^+], 269 (10 %), 218 (25 %), 91 (45 %), 77 (5 %), 63 (22 %), 52 (18 %), 41 (11 %)

2-Nitro-4-iodoaniline (Figure 9)

GC-MS (EI, 70 eV): m/z (%) = 264 (100 %) [M^+], 234 (10 %), 218 (30 %), 107 (8 %), 91 (45 %), 63 (20 %), 52 (17 %)

3-Nitro-4-iodoaniline (Figure 10)

GC-MS (EI, 70 eV): m/z (%) = 264 (100 %) [M^+], 234 (10 %), 218 (28 %), 206 (10 %), 151 (20 %), 91 (95 %), 64 (29 %), 52 (30 %)

4-Nitro-2-iodoaniline (Figure 11)

GC-MS (EI, 70 eV): m/z (%) = 264 (100 %) [M^+], 234 (50 %), 218 (10 %), 91 (80 %), 63 (26 %).

3-Chloro-4-iodoaniline (Figure 12)

GC-MS (EI, 70 eV): m/z (%) = 255 (33 %) [M^+], 253 (100 %), 128 (15 %), 126 (50 %), 99 (28 %), 90 (25 %), 63 (30 %).

4-Chloro-2-iodo-aniline (Figure 13)

GC-MS (EI, 70 eV): m/z (%) = 255 (33 %) [M^+], 253 (100 %), 128 (15 %), 126 (45 %), 101 (5 %), 99 (23 %), 90 (25 %), 63 (27 %), 52 (8 %).

4-Iododiphenyl amine (Figure 14)

GC-MS (EI, 70 eV): m/z (%) = 295 (100 %) [M^+], 167 (60 %), 139 (15 %), 121 (5 %), 84 (20 %), 65 (5 %), 51 (7 %).

4-Iododiphenyl ether (Figure 15)

GC-MS (EI, 70 eV): m/z (%) = 296 (100 %) [M^+], 141 (45 %), 115 (35 %), 92 (7 %), 77 (25 %), 63 (13 %), 51 (15 %)

4-Iodo-*N,N*-Dimethylaniline (Figure 16)

GC-MS (EI, 70 eV): m/z (%) = 247 (100 %) [M^+], 231 (5 %), 119 (20 %), 105 (10 %), 91 (5 %), 77 (12 %), 63 (8 %), 42 (13 %)

4-Methyl-2-iodoaniline (Figure 17)

GC-MS (EI, 70 eV): m/z (%) = 234 (5 %) [M^+], 107 (3 %), 102 (5 %), 89 (18 %), 87 (73 %), 75 (8 %), 58 (25 %), 45 (100 %), 43 (95).

4-iodo-anisole (Figure 18)

GC-MS (EI, 70 eV): m/z (%) = 234 (7 %) [M^+], 107 (17 %), 88 (20 %), 75 (10 %), 71 (100 %), 58 (70 %).

4-methyl-2-iodo-phenol (Figure 19)

GC-MS (EI, 70 eV): m/z (%) = 234 (100 %) [M^+], 107 (50 %), 77 (40 %), 51 (20 %).

4-Tert-butyl-2-iodophenol (Figure 20)

GC-MS (EI, 70 eV): m/z (%) = 276 (28 %) [M^+], 261 (100 %), 233 (8 %), 134 (30 %)

2-Hydroxy-5-iodobenzaldehyde (Figure 21)

GC-MS (EI, 70 eV): m/z (%) = 248 (100 %) [M^+], 229 (6 %), 219 (8 %), 92 (8 %), 75 (10 %), 65 (23 %), 45 (37 %)

4-chloro-2-iodo-phenol (Figure 22)

GC-MS (EI, 70 eV): m/z (%) = 255 (30 %) [M^+], 254 (100 %), 127 (30 %), 99 (40 %), 63 (39 %).

2, 4-dichloro-6-iodo-phenol (Figure 23)

GC-MS (EI, 70 eV): m/z (%) = 289 (60 %) [M^+], 288 (100 %), 161 (10 %), 133 (40 %), 97 (35 %), 73 (10 %), 62 (30 %).

2,2,4-trimethyl-1,2-dihydroquinoline (Figure 25)

GC-MS (EI, 70 eV): (Figure 4.38) m/z (%) = 173 (9 %) [M^+], 158 (100 %), 143 (7 %), 115 (8 %)

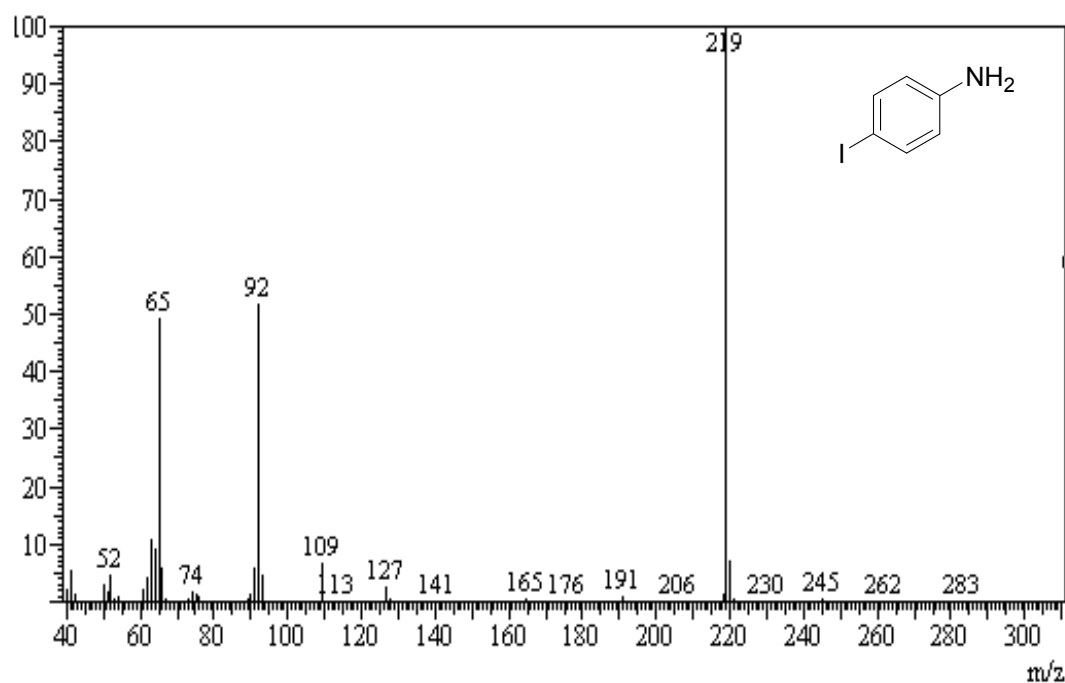


Figure 7. Mass spectrum of 4-iodoaniline

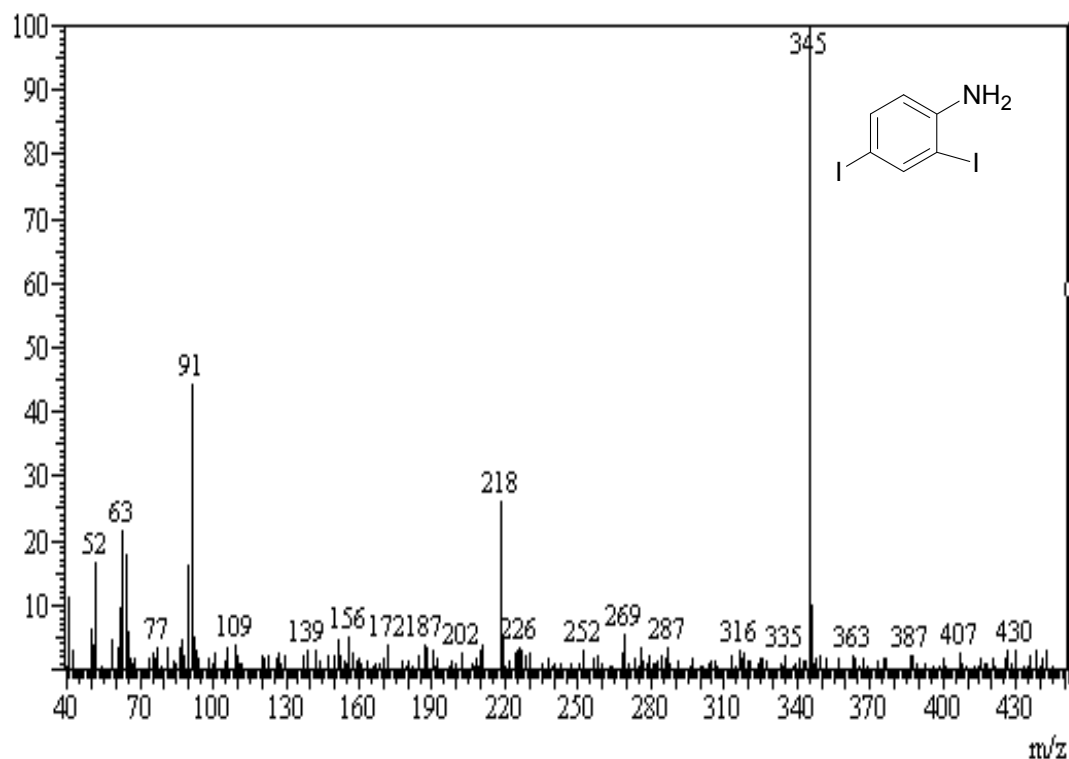


Figure 8. Mass spectrum of 2,4-diiodoaniline

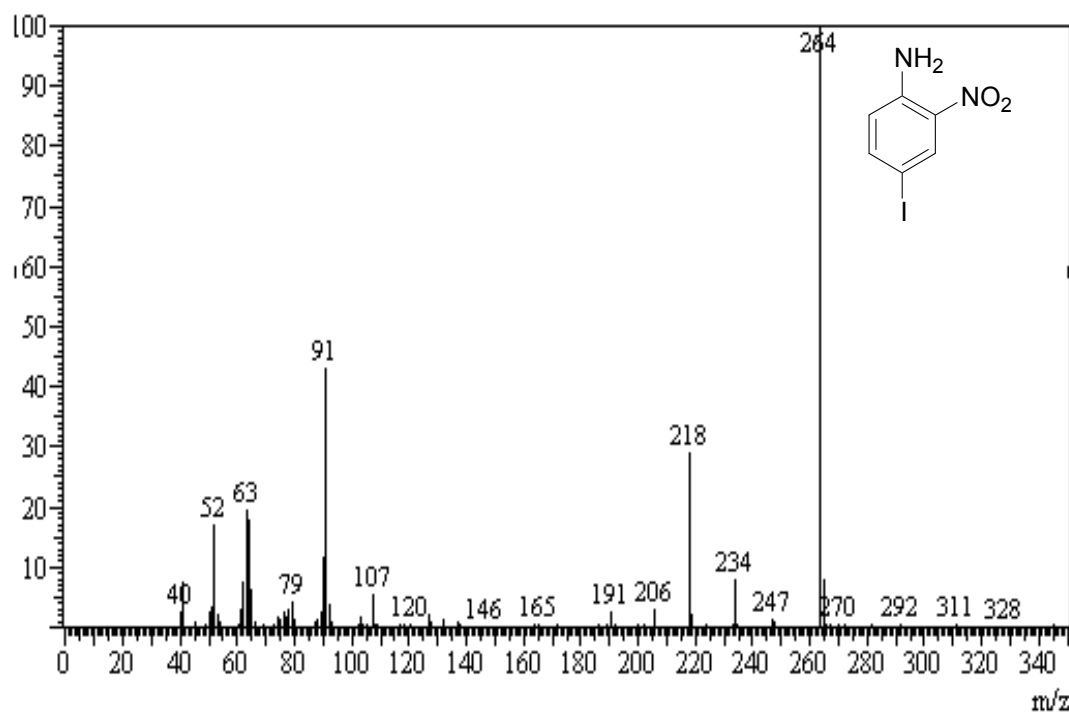


Figure 9. Mass spectrum of 2-nitro-4-iodoaniline

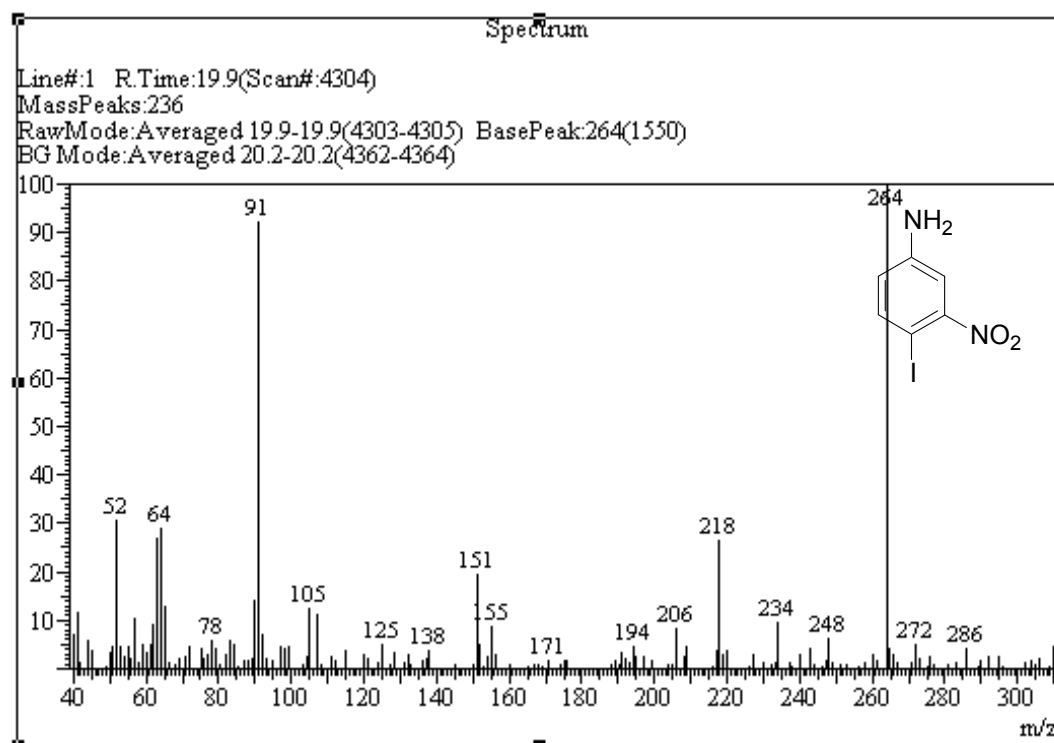


Figure 10. Mass spectrum of 3-nitro-4-iodoaniline

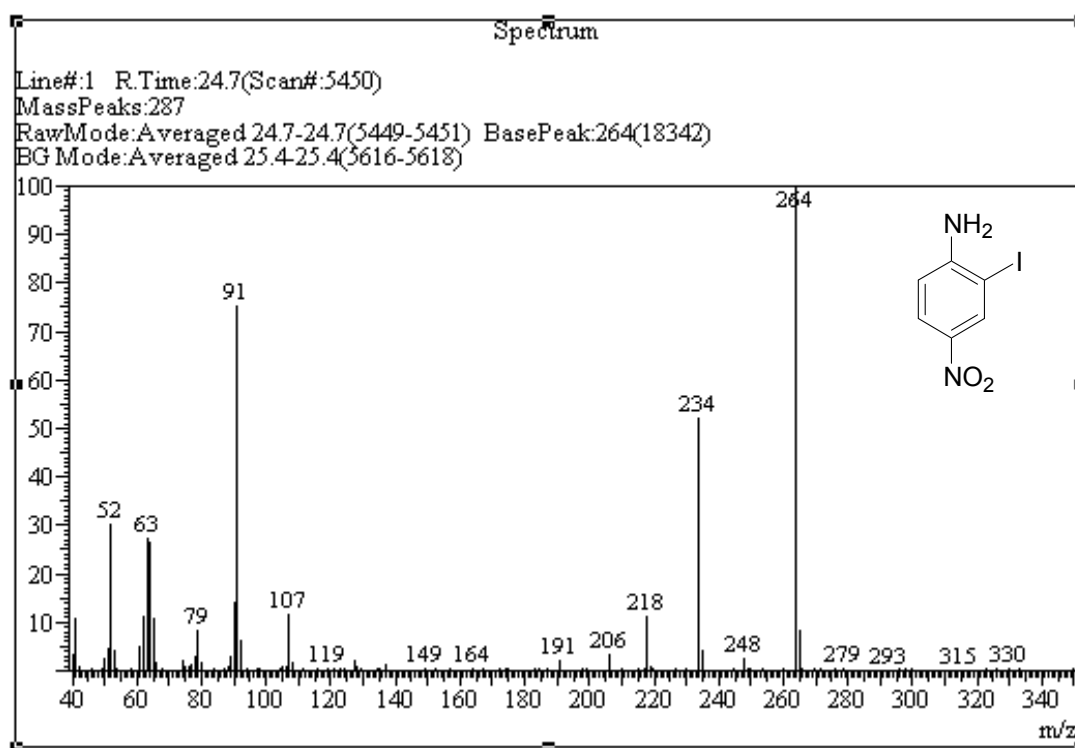


Figure 11. Mass spectrum of 4-nitro-2-iodoaniline

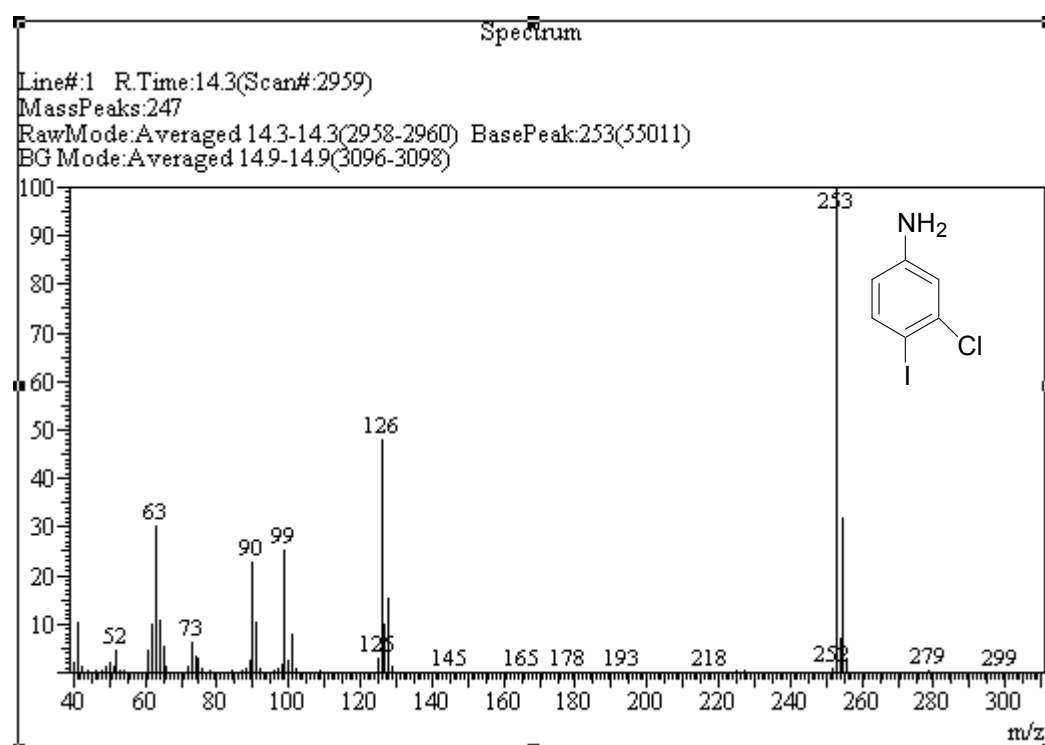


Figure 12. Mass spectrum of 3-Chloro-4-iodoaniline

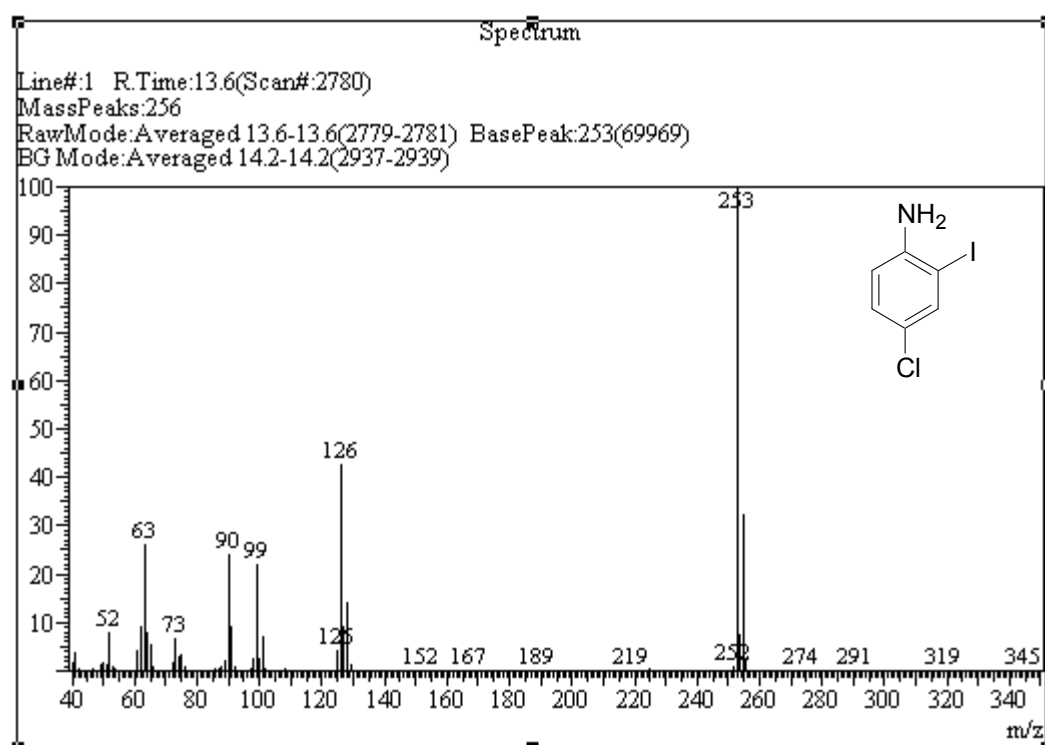


Figure 13. Mass spectrum of 4-Chloro-2-iodoaniline

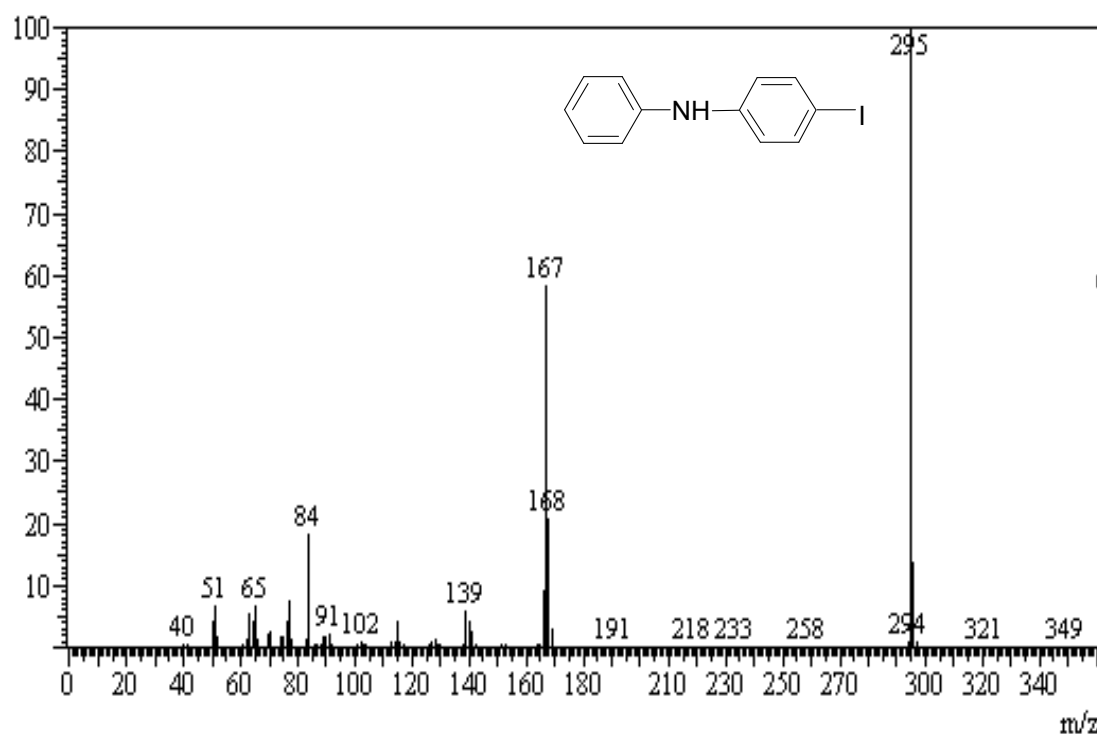


Figure 14. Mass spectrum of 4-iodo-*N*-phenylaniline

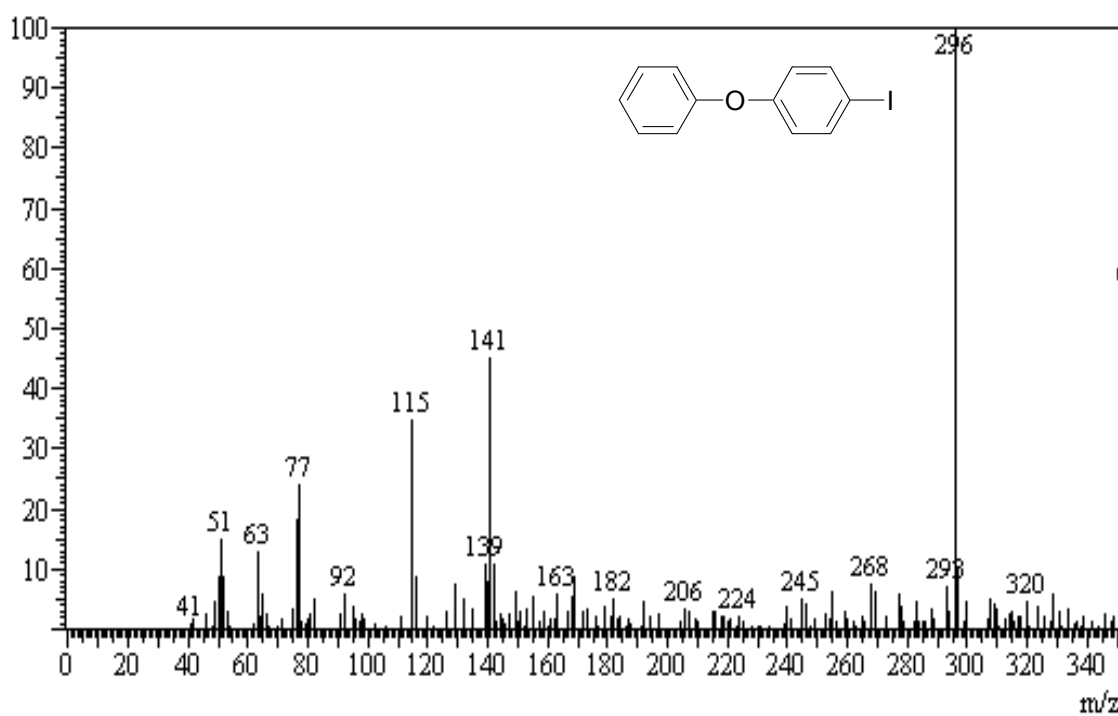


Figure 15. Mass spectrum of 4-iododiphenyl ether

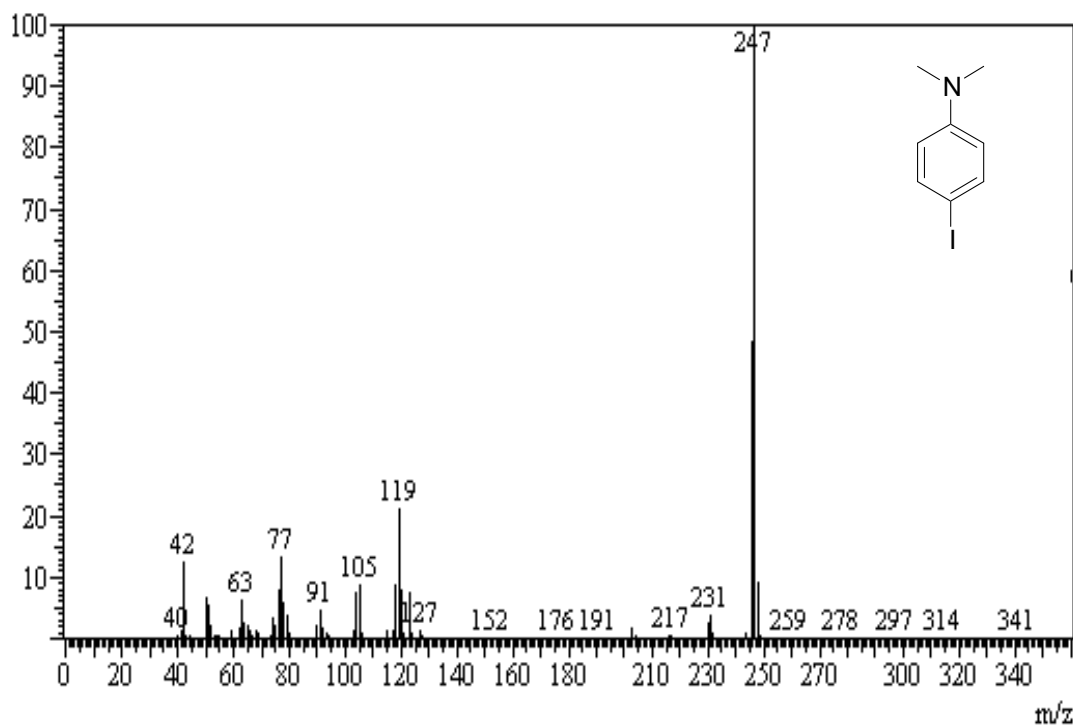


Figure 16. Mass spectrum of 4-iodo-*N,N*-dimethylbenzenamine

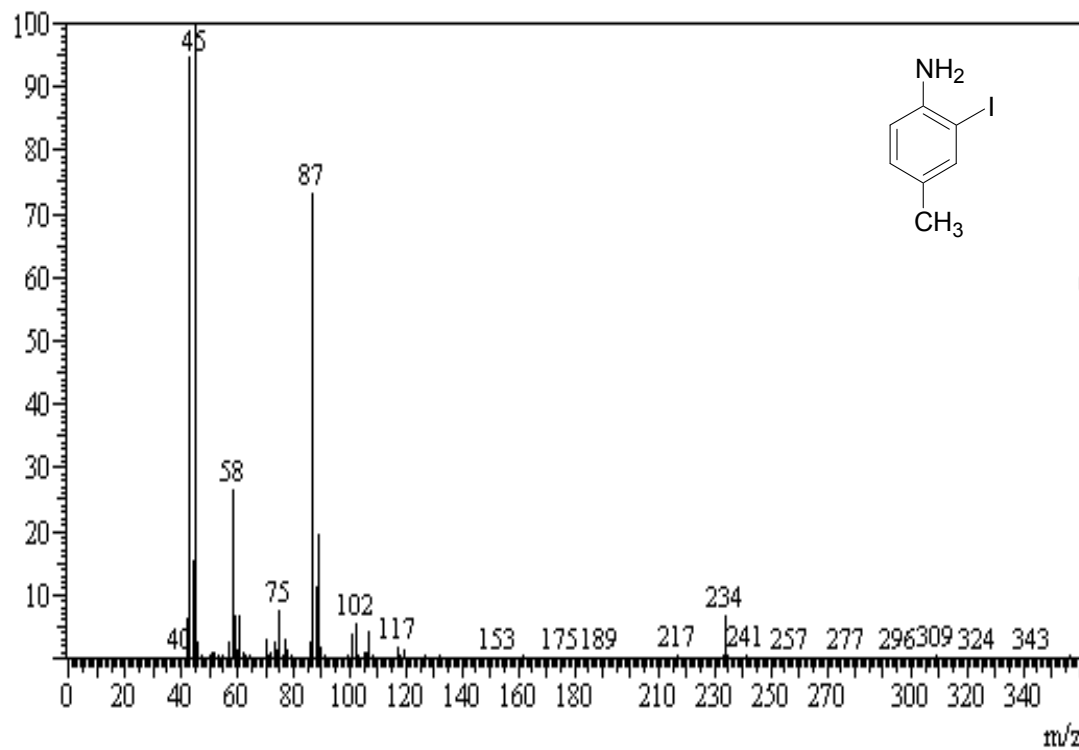


Figure 17. Mass spectrum of 2-iodo-4-methylaniline

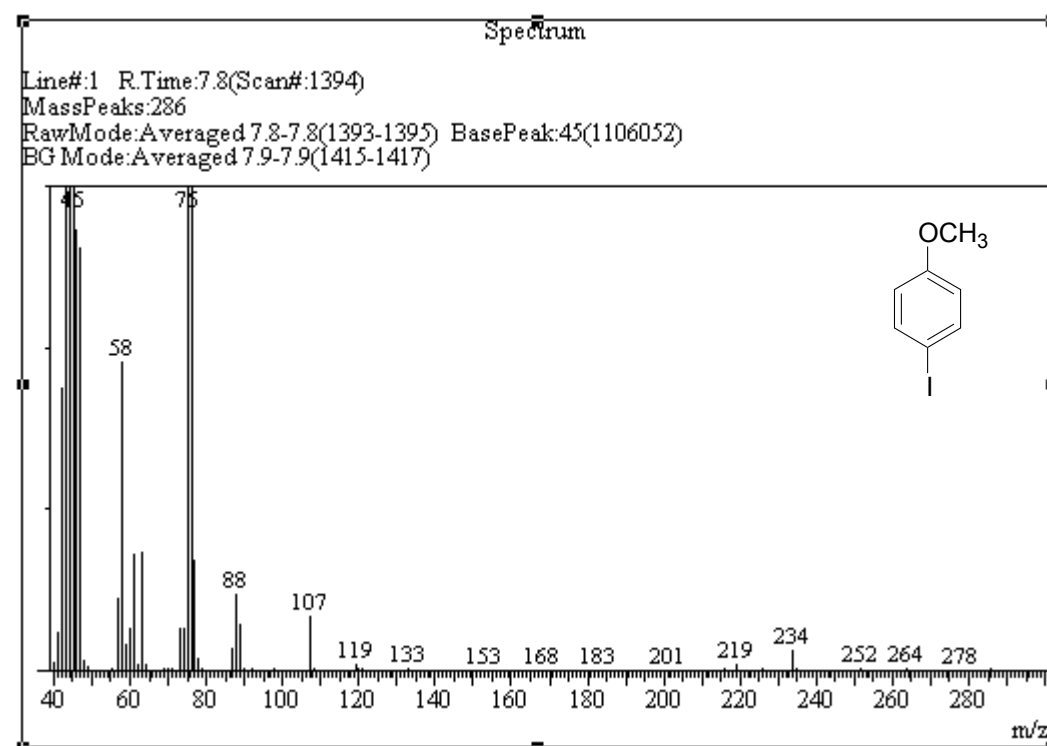


Figure 18. Mass spectrum of 4-iodo-anisole

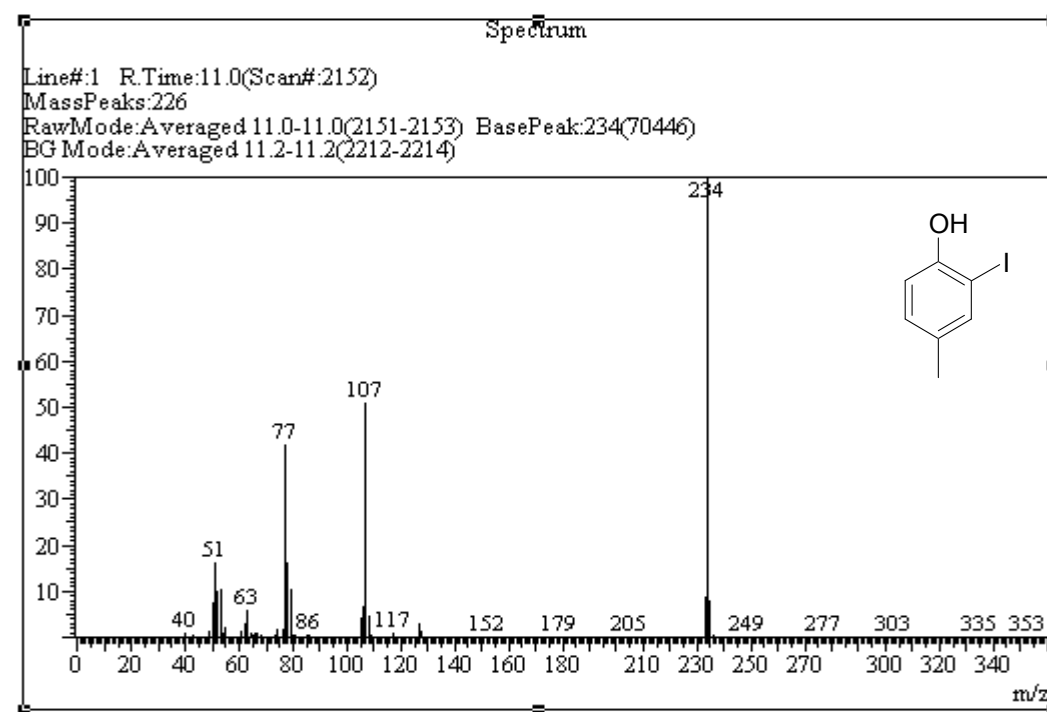
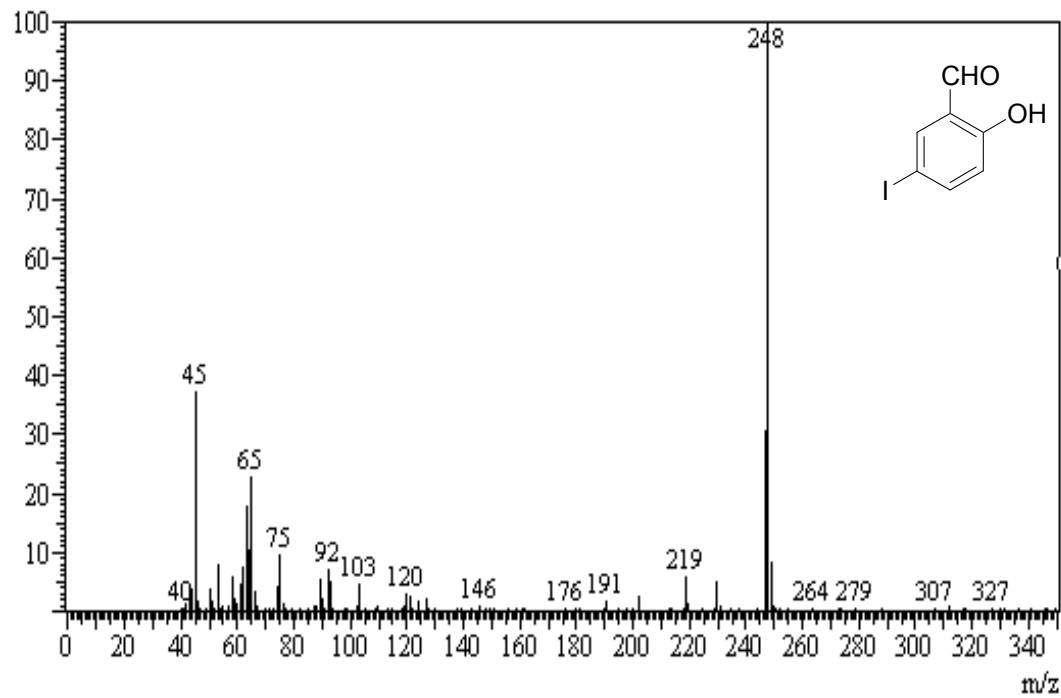


Figure 19. Mass spectrum of 4-methyl-2-iodo-phenol



Figure

20. Mass spectrum of 2-hydroxy-5-iodobenzaldehyde

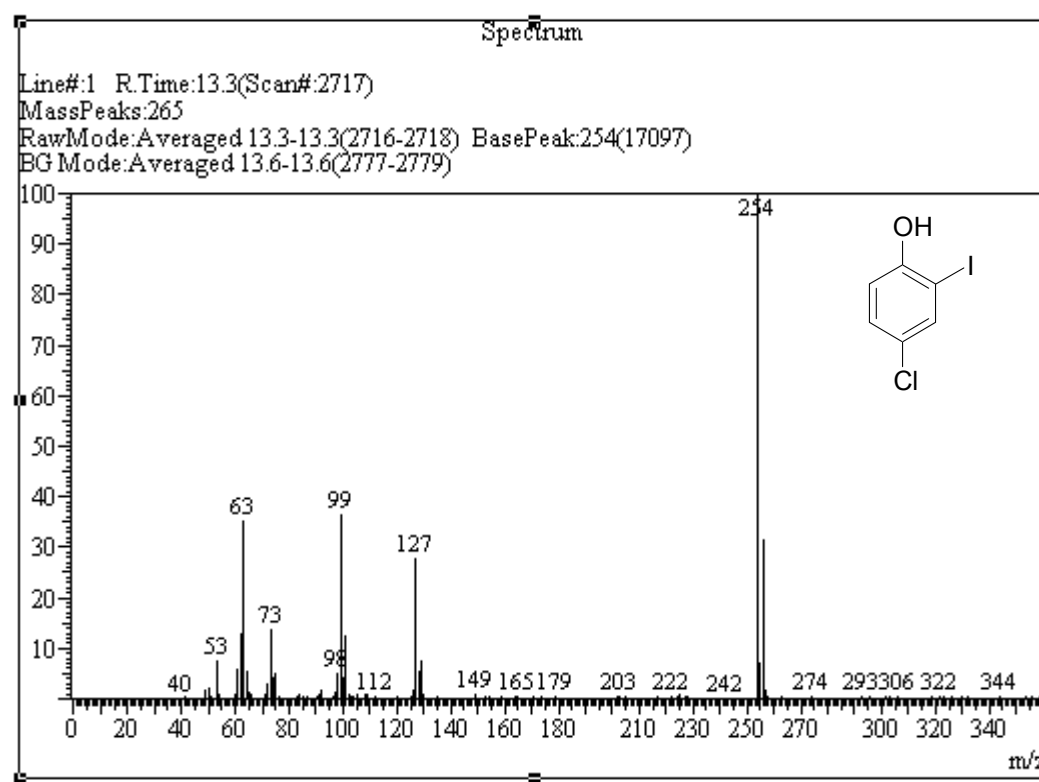


Figure 21. Mass spectrum of 4-chloro-2-iodo-phenol

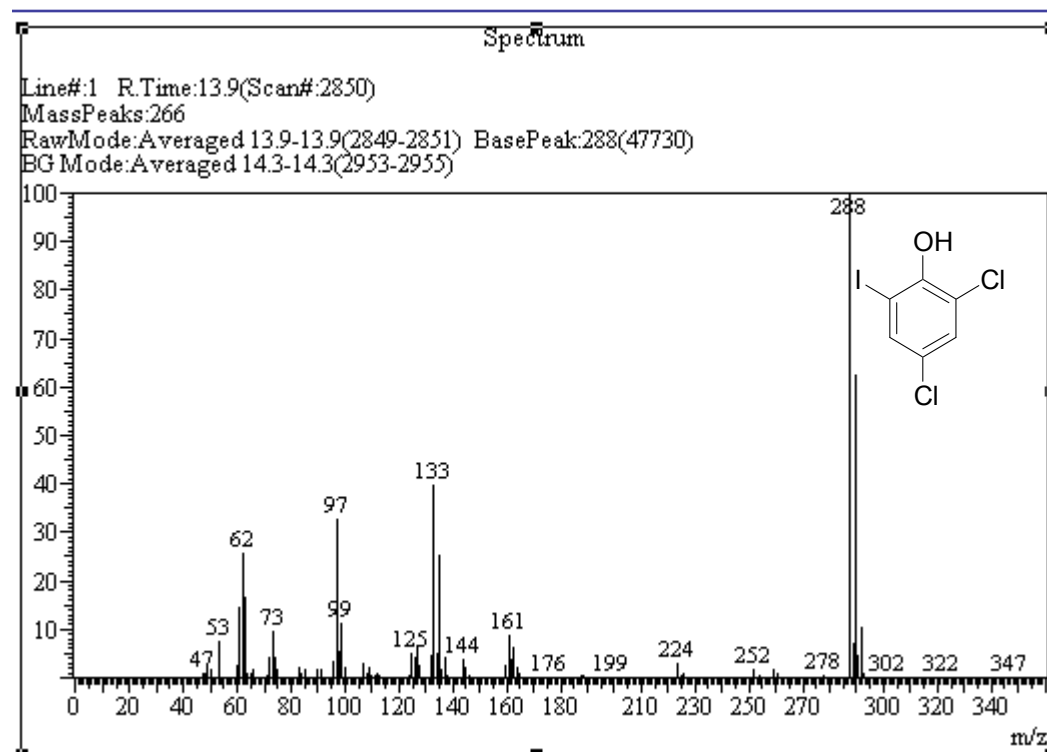


Figure 22. Mass spectrum of 2,4 dichloro-4-iodophenol

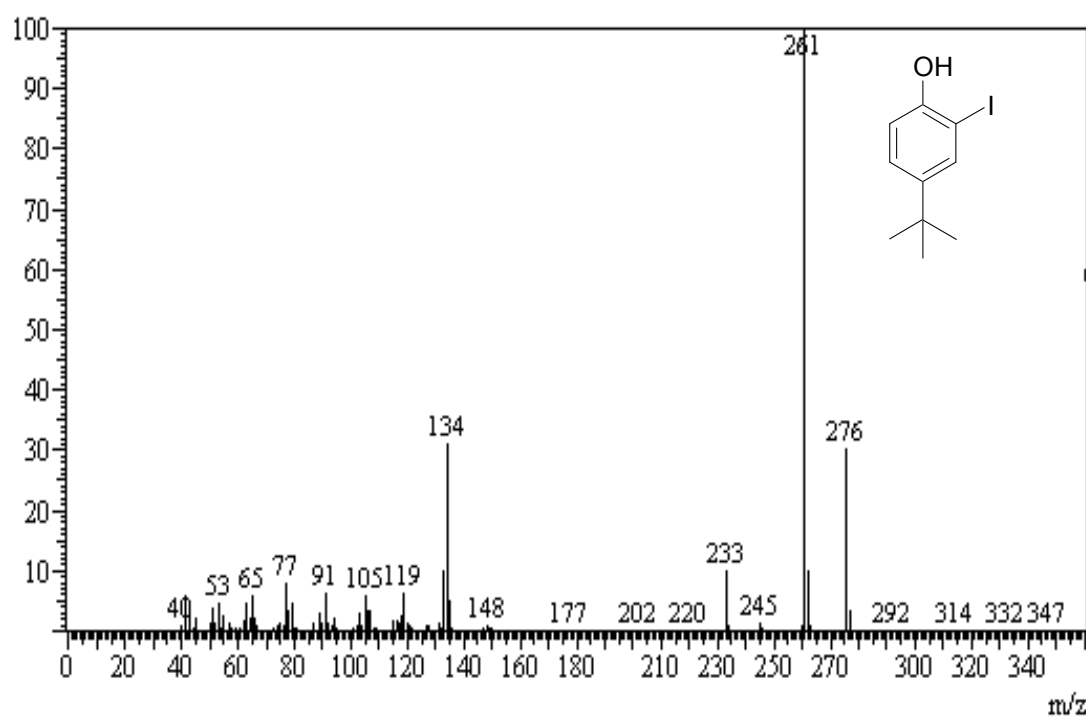


Figure 23. Mass spectrum of 4-*tert*-butyl-2-iodophenol

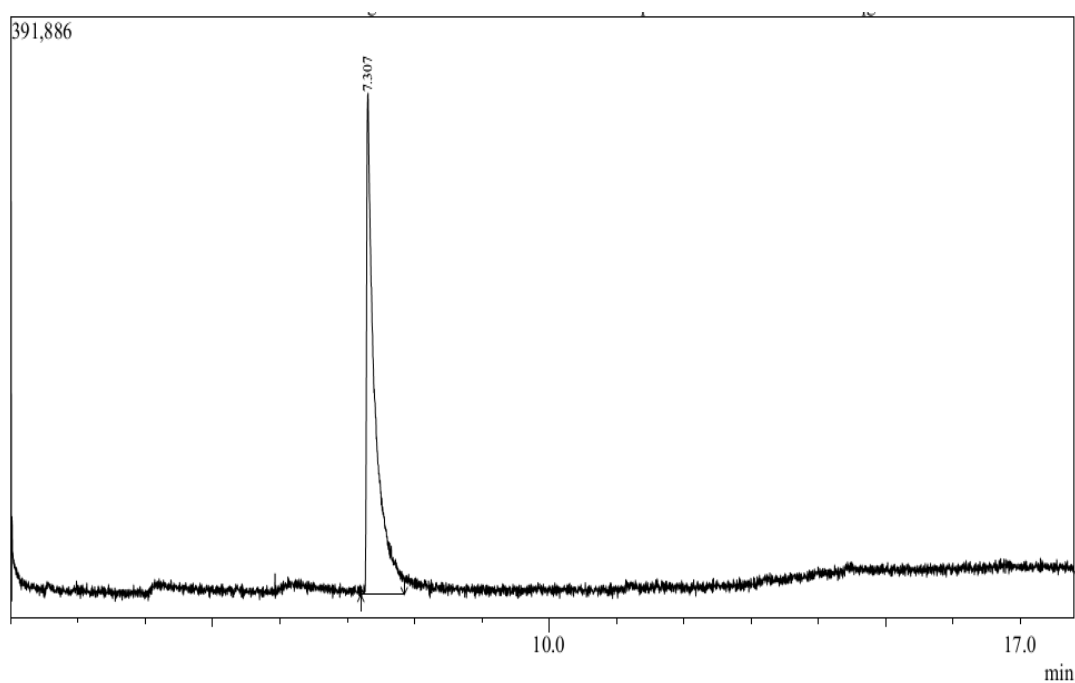


Figure 24. Gas Chromatogram of 2,2,4-trimethyl-1,2-dihydroquinoline (**R.T-7.30 min**).

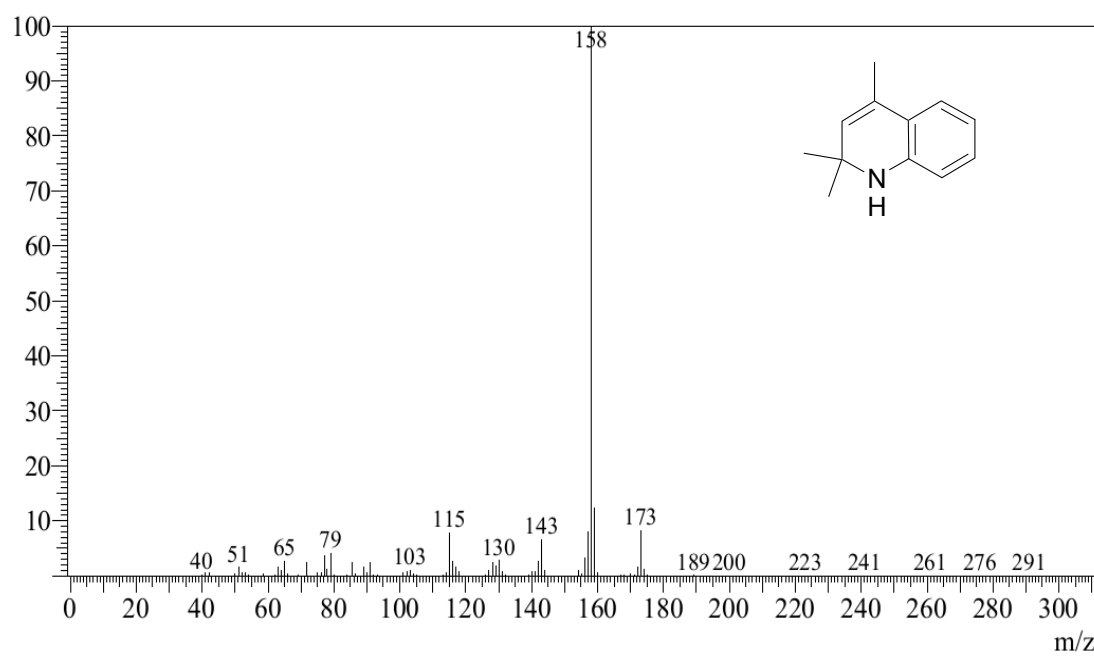


Figure 25. Mass spectrum of 2,2,4-trimethyl-1,2-dihydroquinoline

References':

- 1.J. R. Sohn, S. H. Lee and J. S. Lim, *Catalysis Today* 2006, **116**, 143–150.
- 2.J. R. Sohn, J. S. Lim S. H. Lee, *Chemistry Letters* 2004, **33**, 1490-1491
- 3.N. Kaneniwa, A. Ikekawa, H. Hayase, *Chem. Pharma. Bull.* 1974, **22**, 11, 2635-2641.